EXPERIMENTAL CELL RESEARCH 319 (2013) 487–497

Available online at www.sciencedirect.com

SciVerse ScienceDirect

journal homepage: www.elsevier.com/locate/yexcr

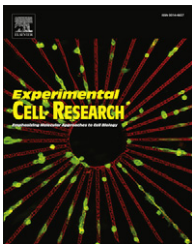

Research Article

Directional cell migration in an extracellular pH gradient: A model study with an engineered cell line and primary microvascular endothelial cells

Ranjani K. Paradise[a], *Matthew J. Whitfield*[b], *Douglas A. Lauffenburger*[a], *Krystyn J. Van Vliet*[a,b,*]

[a]*Department of Biological Engineering, Massachusetts Institute of Technology, Cambridge, MA 02139, USA*
[b]*Department of Materials Science and Engineering, Massachusetts Institute of Technology, Cambridge, MA 02139, USA*

ARTICLE INFORMATION

Article Chronology:
Received 8 August 2012
Received in revised form
3 November 2012
Accepted 5 November 2012
Available online 12 November 2012

Keywords:
Cell migration
Extracellular pH gradient
Integrin-activation
Tumor
Wound healing

ABSTRACT

Extracellular pH (pH_e) gradients are characteristic of tumor and wound environments. Cell migration in these environments is critical to tumor progression and wound healing. While it has been shown previously that cell migration can be modulated in conditions of spatially invariant acidic pH_e due to acid-induced activation of cell surface integrin receptors, the effects of pH_e gradients on cell migration remain unknown. Here, we investigate cell migration in an extracellular pH_e gradient, using both model $\alpha_v\beta_3$ CHO-B2 cells and primary microvascular endothelial cells. For both cell types, we find that the mean cell position shifts toward the acidic end of the gradient over time, and that cells preferentially polarize toward the acidic end of the gradient during migration. We further demonstrate that cell membrane protrusion stability and actin–integrin adhesion complex formation are increased in acidic pH_e, which could contribute to the preferential polarization toward acidic pH_e that we observed for cells in pH_e gradients. These results provide the first demonstration of preferential cell migration toward acid in a pH_e gradient, with intriguing implications for directed cell migration in the tumor and wound healing environments.

© 2012 Elsevier Inc. All rights reserved.

Introduction

It is well known that the average extracellular pH (pH_e) in tumors and wounds is often more acidic than in normal tissues [1–8]. Tumors and wounds tend to be hypoxic, due to regions of damaged or irregular vasculature, resulting in anaerobic cellular metabolism and production of lactic acid [4,8,9]. Even in regions with sufficient oxygen, alterations in gene expression cause cancer cells to increase reliance on anaerobic metabolism, a phenomenon known as the Wartburg effect [8,10–12]. As glycolysis is an inefficient means of ATP production, cancer cells must increase the rate of glucose consumption and metabolism in order to maintain sufficient energy levels, which accelerates acid production [4]. However, although the average extracellular pH in these contexts is generally acidic, the pH_e environment is not spatially uniform. Rather, high resolution methods for measuring pH_e have shown significant spatial variations in pH_e profiles within tumors [3,13]. For example, pH_e gradients exist within tumors, with pH_e decreasing about 0.7 units

Abbreviations: pH_e, Extracellular pH; MVECs, Microvascular endothelial cells; AIAC, Actin–integrin adhesion complex; NHE1, Na^+/H^+ ion exchanger

*Corresponding author.
E-mail address: krystyn@mit.edu (K.J. Van Vliet).

0014-4827/$ - see front matter © 2012 Elsevier Inc. All rights reserved.
http://dx.doi.org/10.1016/j.yexcr.2012.11.006

(~7.4 to ~6.7) over ~350 μm from a tumor blood vessel for human colon adenocarcinoma xenografts [13]. Furthermore, pH_e gradients have been measured at the interfaces between tumors and normal tissue, with pH_e increasing about 0.4 units (~6.9 to ~7.3) over 1 mm toward the normal tissue for human prostate tumors grown in mice [4]. Although pH_e profiles have not been measured in the wound context, the presence of oxygen gradients at wound sites implies that pH_e gradients occur in these environments as well [14–16]. Finally, in addition to gradients that span many cell lengths, pH_e gradients can also exist at the single cell level, due to localization of the Na^+/H^+ ion exchanger NHE1 to the leading edge of migrating cells [17].

It is possible that pH_e gradients could alter migration of cells that are involved in tumor growth and wound healing. Cell migration is generally mediated by binding interactions between transmembrane integrin receptors and extracellular matrix (ECM) ligands. We have previously shown that acidic pH_e promotes conversion of integrin $\alpha_v\beta_3$ to a high-affinity conformation, a process known as integrin activation, and that this can modulate cell migration in conditions of spatially uniform acidic pH_e by increasing the overall adhesiveness to the surrounding ECM [18]. However, cell migration in pH_e gradients has not yet been explored.

Studies with fibronectin surface gradients have demonstrated that cells preferentially migrate toward higher fibronectin coating concentrations, which have higher adhesiveness due to higher spatial density of adhesive ligands [19,20]. In the context of our previous work, this suggests that cells in a pH_e gradient may preferentially migrate toward lower pH_e. This could be particularly important for microvascular endothelial cells migrating within or toward tumors or wounds to initiate vascularization in hypoxic areas.

Here, we establish gradients from pH_e 6.0–7.5 and investigate the migration of model $\alpha_v\beta_3$ CHO-B2 cells and primary bovine retinal microvascular endothelial cells (MVECs) in the pH_e gradients. We examine the former engineered cell type first because this cell line exhibits a relatively well characterized integrin/fibronectin interaction, and then we validate the findings using the latter, more physiologically relevant cell type. We observe that mean cell position moves progressively toward lower pH_e over time for both cell types. We then discuss possible mechanisms underlying this shift in mean cell position with additional experiments and the aid of a computational cell migration model. We find that MVECs exhibit direction-dependent migration velocity, with cells oriented toward acid migrating faster than cells oriented away from acid. Additionally, both $\alpha_v\beta_3$ CHO-B2 cells and MVECs polarize preferentially toward lower pH_e during migration. Finally, we find that cells in acidic pH_e have longer membrane protrusion lifetimes and more actin–integrin adhesion complexes than cells in pH_e 7.4, which may contribute to regulation of directionality during cell migration in pH_e gradients.

Materials and methods

Cell culture and experimental solutions

$\alpha_v\beta_3$ CHO-B2 cells were provided by Dr. L. Griffith (Massachusetts Institute of Technology), as subcultures of a cell line developed by Dr. J. Schwarzbauer (Princeton University) and Dr. S. Corbett (University of Medicine and Dentistry of New Jersey). Cell culture media for $\alpha_v\beta_3$ CHO-B2 cells consisted of high-glucose bicarbonate-buffered Dulbecco's Modified Eagle Medium (DMEM) (Invitrogen) containing L-glutamine and sodium pyruvate, supplemented with 10% fetal bovine serum (Hyclone), 1% antibiotics-antimyotics (Invitrogen), 1% non-essential amino acids (Invitrogen), and 500 μg/mL zeocin (Invitrogen). Bovine retinal microvascular endothelial cells were provided by Dr. I. Herman (Tufts University). Cell culture media for MVECs consisted of low-glucose bicarbonate-buffered DMEM containing L-glutamine and sodium pyruvate, supplemented with 10% bovine calf serum (Sigma) and 12.5 mM HEPES (Sigma). Both cell types were maintained in an incubator at 37 °C with 5% CO_2 and, unless otherwise noted, all cell incubations occurred under these conditions.

For cell migration, kymography, and actin–integrin adhesion complex imaging experiments, a serum and bicarbonate free version of the cell specific media described above was used. Bicarbonate-free media enabled precise control of pH during the course of experiments and has been used previously for many cell types [17, 21–25]. The pH in bicarbonate-free media was adjusted using 1 M HCl or NaOH. For a discussion of bicarbonate-free versus bicarbonate-buffered environment see the Discussion and conclusions.

Dunn chamber setup and extracellular pH gradient imaging

The Dunn chamber (Hawksley) was set up according to the manufacturer's instructions. Briefly, both wells were filled with bicarbonate-free serum-free media at pH 7.5 and covered with a coverslip, leaving a thin slit open at the outer well. The sides of the coverslip, but not the slit, were sealed to the chamber slide using a melted wax mixture consisting of 1:1:1 paraffin:beeswax:Vaseline, and the outer well was drained with a Kimwipe. The outer well was then filled with bicarbonate-free serum-free pH 6.0 media using a syringe, and the slit was sealed with the melted wax mixture. For gradient imaging, 10 μM BCECF (2′,7′-bis-(2-carboxyethyl)-5-(and -6)-carboxyfluorescein) (Invitrogen) was added to the bicarbonate-free serum-free $\alpha_v\beta_3$ CHO-B2 cell media. The bridge region was imaged at 4× magnification at excitation wavelengths of ~440 nm and ~495 nm, both with an emission wavelength of ~535 nm. The ratio of the 495/440 nm light intensities is linear with pH. To assess gradient stability, images were taken every hour over 8 h for chambers at 37 °C, and two independent experiments were conducted. Data points near the edges of the bridge were excluded due to artifacts in light intensity.

Cell migration measurements

Number 2 glass coverslips were coated with 30 μg/ml human plasma fibronectin (Sigma) in phosphate buffered saline (PBS) at pH 7.4 for 1 h at room temperature, then rinsed twice with PBS. Cells were plated on coverslips in serum-free media and allowed to adhere for 2–3 h before being placed in the Dunn chamber. Media loaded into the Dunn chamber wells consisted of bicarbonate-free serum-free media, and chambers were set up as described above. Cells were imaged at 4× magnification every

5 min for 8 h in an incubator at 37 °C. For each cell over the bridge region, images were rotated such that the gradient was oriented vertically, with the acidic end at the top of the image. For cells over the center post, images were rotated in a similar manner, such that a line drawn from the middle of the post through the cell was oriented vertically in the images, with the outside edge of the post at the top of the image. Rotation for all images in the time-lapse stack for each cell was based on the cell position at time 0. The initial position of each cell was set to the origin at (0,0) before cell tracking. Cell centroids were tracked using ImageJ, and cells that divided, touched other cells, or migrated less than 10 μm from their initial location were excluded from further analysis. After excluding these cells, at least 120 cells in the gradient region were analyzed for each cell type. Mean-squared displacements as a function of time ($<d^2(t)>$) were calculated using the method of non-overlapping intervals [26]. The root mean-squared displacement for the shortest interval was divided by the interval time (5 min) to obtain cell speed. Two or three independent experiments were conducted for each cell type, and data were pooled to obtain percentages and averages shown in figures.

Cell migration model

The numerical model of cell migration used in this paper was modified from a model previously developed by DiMilla et al. [27]. The model was enhanced to include pH_e-dependent integrin activation to enable investigation of the effect of extracellular pH on cell migration. The model consists of two main steps: (1) determination of the steady state receptor distribution within the cell membrane based on receptor diffusion, trafficking, and surface binding; and (2) calculation of cell displacement based on the receptor distribution and internal cell contractile forces. Extensive details of the original model can be found in the DiMilla et al. paper [27], but a brief summary required to understand our modifications and implementation is provided in the Supporting Material and Fig. S1A. Model parameters not obtained from literature or set by our experiments were calibrated to match model output to the mean $\alpha_v\beta_3$ CHO-B2 cell migration speed as a function of pH_e (Supporting material Table S1, Fig. S1B).

Kymography

Glass-bottom 60-mm-diameter Petri dishes (MatTek) were coated with 30 μg/ml fibronectin in PBS at pH 7.4 for 1 h at room temperature and then rinsed twice with PBS. $\alpha_v\beta_3$ CHO-B2 cells were plated on dishes in serum-free media and incubated for 2–3 h before media was changed to bicarbonate-free serum-free media at pH 6.5 or 7.4. Cells were imaged in phase contrast at 40× magnification in an incubator at 37 °C. Three independent experiments comparing pH_e 7.4 and 6.5 were conducted. Independent experiments showed consistent results and data shown in figures is from a single representative experiment. For each experiment, approximately 10–20 cells were imaged and at least 100 individual protrusion events were analyzed for each pH_e condition. Images were collected every 5 s for 25 min. Each kymograph was produced by drawing a one-pixel-wide line perpendicular to the cell membrane at an active membrane region. The images along this line at all time points were then sequentially compiled, illustrating the membrane dynamics at that specific cell location. For each visible protrusion event on a kymograph, a straight line was drawn from the beginning of the event to its peak, or to the beginning of a plateau. Events with a height of less than 4 pixels were neglected. Protrusion lifetime was quantified as the x-axis projection of this line, with the addition of plateau duration, if applicable.

GFP-vinculin transfection

Cells were transfected with GFP-vinculin (provided by Dr. Benjamin Geiger (Weizmann Institute of Science)) according to manufacturer's instructions. Briefly, $\alpha_v\beta_3$ CHO-B2 cells were plated on tissue-culture treated 6-well plates (Falcon) in 2 ml antibiotic-free serum-free media per well. For each well, 1.5 μg plasmid DNA was diluted in 500 μl Opti-MEM (Invitrogen) media and mixed thoroughly. Plus Reagent (Invitrogen) was gently mixed and 1.5 μl was added to the diluted DNA. The solution was mixed gently and incubated for 5 min at room temperature. Next, Lipofectamine (Invitrogen) was gently mixed and 2 μl was added to the diluted DNA. The solution was mixed thoroughly and incubated for 30 min at room temperature. This solution was added dropwise to each well containing cells and gently mixed with cell media. Cells were incubated for 18–24 h and then media was changed to complete growth media. Reagents for bacterial transformation and plasmid amplification were obtained from Dr. Ron Weiss (Massachusetts Institute of Technology).

Actin–integrin adhesion complex imaging

Before imaging, glass bottom 6-well or 12-well plates (MatTek) were coated with 30 μg/ml fibronectin in PBS at 7.4 for 1 h at room temperature and then rinsed twice with PBS. Transfected cells were plated in wells in serum-free media and allowed to adhere for 2–3 h. Media was then changed to bicarbonate-free serum-free media at pH 7.4 or 6.5. Cells were imaged in an incubator at 37 °C at 60× with a GFP filter cube. Three independent experiments were conducted for each duration of exposure to acidic pH_e, and at least 35 cells were imaged for each condition within each experiment. Independent experiments showed consistent results and data shown in figures are from a single representative experiment.

Statistical analysis

To compare mean cell x- and y-coordinates with a null hypothesis of zero, the z-statistic was calculated as: $z = (\hat{x}-\mu_0)/(s/\sqrt{n})$, where $\hat{x}$ is the mean measured coordinate, μ_0 is the expected value of 0, s is the standard deviation of cell position, and n is the number of cells measured. The two-tailed p value was then calculated from a table of standard normal curve areas. To assess dependence of population percentages on cell position, the Marascuilo procedure for multiple comparisons was applied.

To construct 95% confidence intervals for percentage data, a bootstrapping sampling method was used [28]. Briefly, for each set of cell positions at the 8-h timepoint, 10,000 bootstrapped data sets were created by randomly sampling the original data set with replacement. The population percentage that moved in the direction of interest was calculated for each bootstrapped data set. The 95% confidence interval was taken as the range

encompassing the middle 95% of the values calculated for the 10,000 bootstrapped data sets.

Unless otherwise noted, p values for comparison of two conditions were calculated with an unpaired t-test. For comparison of three or more conditions, p values were calculated with a Bonferroni post-test following one-way ANOVA. The Rayleigh test was used to assess angular histograms, with the null hypothesis assuming a uniform distribution.

Results

Migration of $\alpha_v\beta_3$ CHO-B2 cells in an extracellular pH gradient

In order to establish pH_e gradients, we used the Dunn chamber, which consists of two concentric wells separated by a bridge of 20 μm depth and ~1 mm width [29]. When the inner well and outer wells are filled with solutions of different pH, a linear H^+ gradient forms across the bridge. The chamber also contains a post of 20 μm depth at the center of the inner well, which is not exposed to a gradient and serves as a control (Fig. 1A). For our experiments, we established a gradient with cell media between pH_e 6.0–7.5. This 1.5 pH unit gradient over ~1 mm has a similar slope to some gradients reported for tumors in vivo [13]. By imaging the pH_e gradient using the pH-sensitive fluorophore BCECF, we found that the gradient was very stable over an 8-h period, allowing for long-timescale imaging of cell migration in the gradient (Supporting Material text and Fig. S2).

We first assessed the migration behavior of $\alpha_v\beta_3$ CHO-B2 cells in the pH_e gradient. These cells express $\alpha_v\beta_3$ as the only fibronectin-binding integrin [30] and thus are an ideal model system for testing how acid-induced activation of $\alpha_v\beta_3$ affects the directionality and velocity of cells migrating in a pH_e gradient. For each experiment, cells were plated on a fibronectin-coated coverslip, which was used to seal a Dunn chamber with the inner well at pH_e 7.5 and the outer well at pH_e 6.0. A coordinate system was chosen such that increasing y-coordinate values correlated with increasing acidity and the x-axis was perpendicular to the pH_e gradient (Fig. 1B). Cells were imaged over a period of 8 h.

Within the pH_e gradient, $\alpha_v\beta_3$ CHO-B2 cells on average moved progressively toward the acidic end (Fig. 1C). The mean positions were significantly greater than zero for all timepoints after ~3 h ($p<0.05$). In contrast, the mean x-coordinates were not significantly different than zero at any time point, indicating that the cells moved approximately equal amounts in the positive and negative x directions (Fig. 1D). In other words, there was no preferred direction for movement perpendicular to the pH_e gradient. The mean x- and y-coordinates for cells within the center control region were not significantly different than zero at any timepoint (Fig. S3, A and B). Additionally, cells did not migrate in a preferred direction when both the inner and outer chambers were filled with solutions of the same pH (Fig. S3C).

Cells at different locations within the gradient are exposed to different ranges of extracellular pH during migration. To assess the effect of gradient position on directionality and velocity of cell migration, the gradient region was divided into five equal segments, and each cell was assigned to one segment based on its initial position. We calculated the percentage of cells that had moved to a position with lower pH_e after 8 h of migration and found that this percentage did not significantly depend on the cell location within the gradient (Fig. 1E). However, cell migration velocity was dependent on position, as cells located closer to pH_e 6.0 moved significantly more slowly than cells located closer to pH_e 7.5 (Fig. 1F). Thus, initial position within the gradient affected cell velocity but not the directionality of migration.

Migration of bovine retinal microvascular endothelial cells in an extracellular pH gradient

Although $\alpha_v\beta_3$ CHO-B2 cells are an ideal model system to study the role of integrin $\alpha_v\beta_3$ in cell migration, they do not have functional relevance in the tumor or wound healing contexts. Therefore, we next studied the migration behavior of bovine retinal microvascular endothelial cells (MVECs) in a pH_e gradient. These primary cells are relevant to both tumors and wounds, as endothelial cell migration is critical to angiogenesis in these environments. Although MVECs contain a mixed population of fibronectin-binding integrins, it has been shown that expression of $\alpha_v\beta_3$ is higher than expression of $\alpha_v\beta_5$, $\alpha_2\beta_1$, and $\alpha_5\beta_1$ in these cells [31]. Thus, we hypothesized that MVECs would respond to the pH_e gradient in a manner similar to that of $\alpha_v\beta_3$ CHO-B2 cells.

MVEC migration experiments were conducted with the same procedure as described above for $\alpha_v\beta_3$ CHO-B2 cells. For MVECs in the gradient, the mean position of the cells progressively moved toward the acidic end of the gradient (Fig. 2A). The mean y-coordinates at all timepoints after~2.5 h were significantly greater than zero ($p<0.05$), but the mean x-coordinates were not significantly different than zero at any timepoint (Fig. 2B). For cells over the center control post, the mean coordinates were also not significantly different than zero at any timepoint (Fig. S3, D and E).

The effects of cell location within the gradient on directionality and velocity were similar to those observed with $\alpha_v\beta_3$ CHO-B2 cells. The percentage of cells that had moved to a final position with lower pH_e after 8 h did not significantly depend on the initial cell location within the gradient (Fig. 2C). However, cell migration speed was significantly slower for cells that were located closer to pH_e 6.0 than for cells located closer to pH_e 7.5 (Fig. 2D). Overall, MVECs exhibited comparable behavior to $\alpha_v\beta_3$ CHO-B2 cells within the pH gradient.

Possible mechanisms for the shift in mean cell position toward lower pH_e

Our cell migration measurements demonstrated that both $\alpha_v\beta_3$ CHO-B2 cells and MVECs on average moved toward the acidic end of the pH_e gradient over time. We have hypothesized three independent possible physical mechanisms for how the pH_e gradient could cause the mean cell position to shift toward lower pH_e. These mechanisms, described in the following sections, consider the effects of the gradient on cell velocity as well as on cell polarization direction, which is defined here as the direction of leading edge extension during migration. We assessed the mechanisms using experimental data, as well as a computational cell migration model that we adapted from DiMilla et al. [27] to now include pH_e-dependent integrin activation. We simulated cells of ~50 μm length within a pH_e gradient of 7.5 to 6.0 over a width of 1 mm such that, as in our experiments, the gradient across any given cell was smaller than

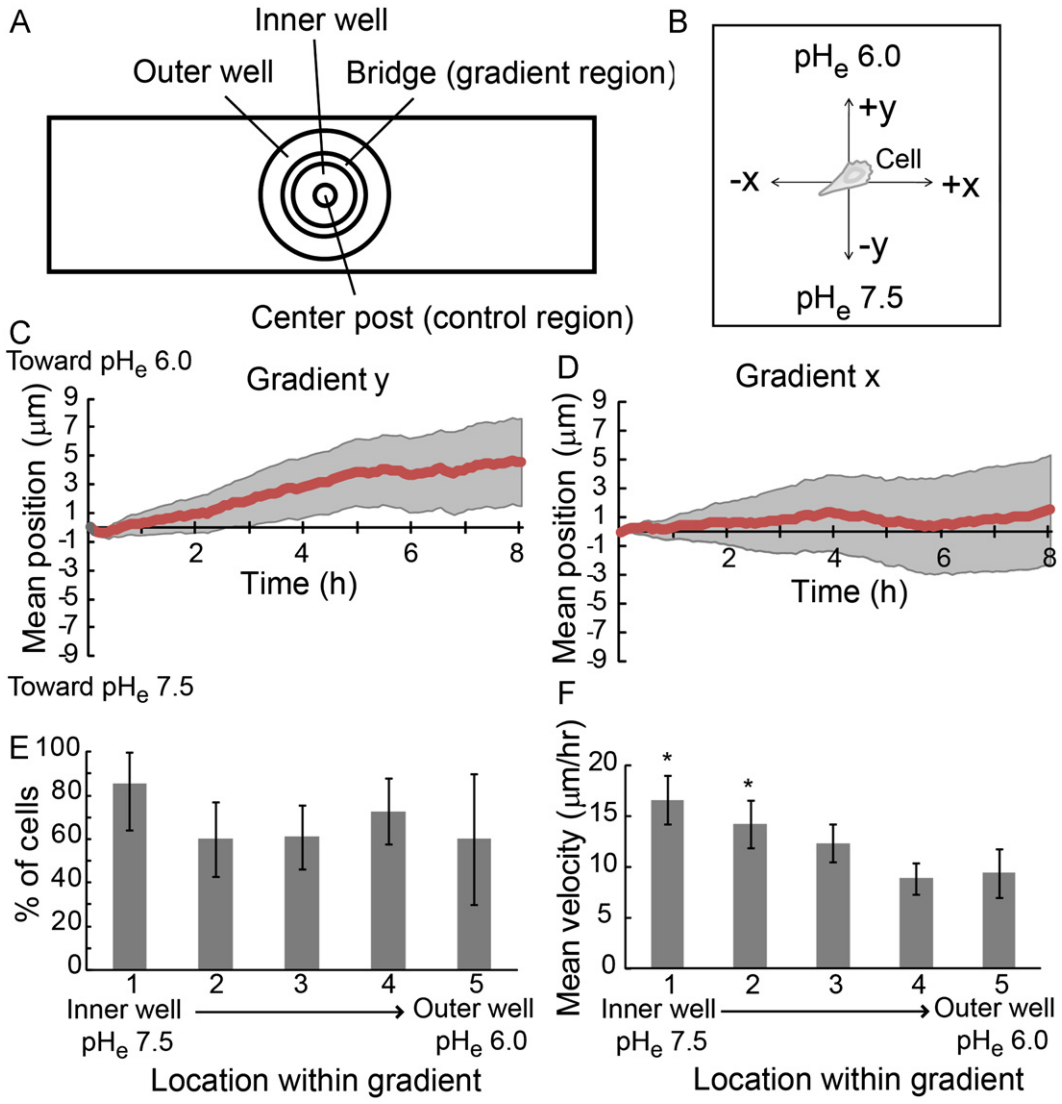

Fig. 1 – Migration of $\alpha_v\beta_3$ CHO-B2 cells in a pH_e gradient. (A) Schematic top-down illustration of the Dunn chamber used to establish pH_e gradients. When the inner and outer wells are filled with solutions of different concentrations, a linear concentration gradient forms across the bridge. (B) Illustration of the coordinate system used for data analysis. For cells in the pH_e gradient, the *y*-axis is parallel to the gradient direction and the *x*-axis is perpendicular to the gradient direction. (C) Mean *y*-coordinate (line) with 95% CI (gray shaded regions) over time for $\alpha_v\beta_3$ CHO-B2 cells in the pH_e gradient. The mean *y*-coordinate is significantly different than zero for all timepoints at which the error bars do not encompass the *x*-axis. (D) Mean *x*-coordinate (line) with 95% CI (gray shaded regions) over time for $\alpha_v\beta_3$ CHO-B2 cells in the pH_e gradient. The mean *x*-coordinate is not significantly different than zero at any timepoint. (E) Percentage of $\alpha_v\beta_3$ CHO-B2 cells in the pH_e gradient that attained a position with positive *y*-coordinate at the 8-h timepoint as a function of cell location within the gradient. No significant dependence on position was observed. (F) Mean $\alpha_v\beta_3$ CHO-B2 cell velocity as a function of cell location within the gradient. Cells closer to pH_e 7.5 moved significantly faster than those closer to pH_e 6.0. Asterisk at location 1 indicates $p<0.05$ with respect to locations 4 and 5. Asterisk at location 2 indicates $p<0.05$ with respect to location 4. Error bars are 95% CI.

the overall gradient of 1.5 units. During each simulation time step, the cell contracts and cell displacement occurs if there is sufficient asymmetry in the ratio of adhesiveness to contractility between the leading and trailing ends of the cell. This migration model allows us to isolate parameters such as polarization direction and leading to trailing edge integrin bond asymmetry in ways not possible in experiments. The model can be used to test the first two mechanisms but not the third, because a pH_e-mediated mechanism for changing polarization direction is not included in the model framework.

Cells become trapped in acidic regions due to decreased migration velocity at lower pH_e

One potential mechanism for the shift in mean cell position is illustrated in Fig. 3A. For both $\alpha_v\beta_3$ CHO-B2 cells and MVECs, cells migrating in more acidic regions of the gradient displayed significantly reduced migration speed. Because of this pH_e-dependent velocity, it is possible that cells could be migrating with no preferred direction, but cells that encounter regions of lower pH_e become effectively trapped there due to decreased migration speed. By this mechanism, the mean cell position

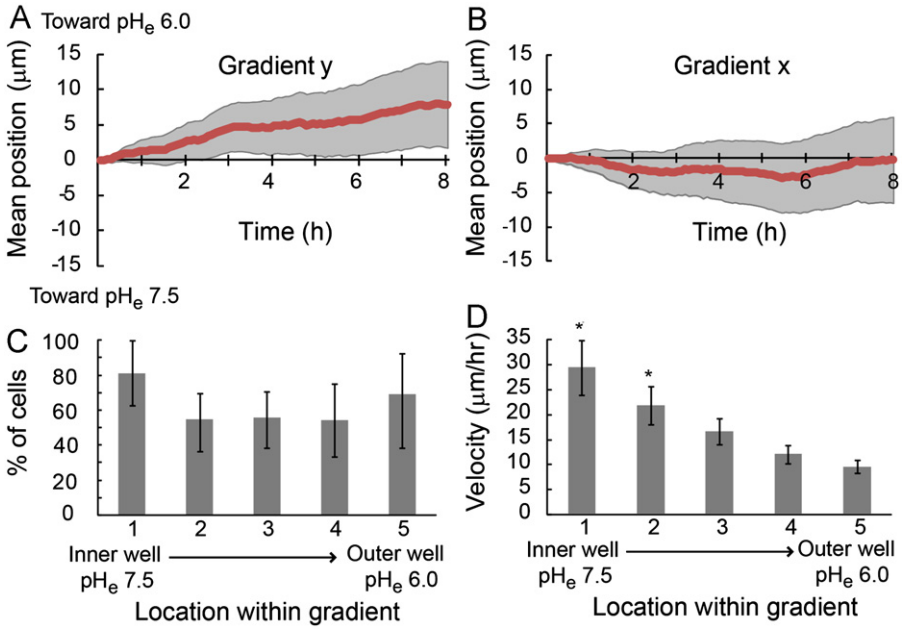

Fig. 2 – Migration of MVECs in a pH$_e$ gradient. (A) Mean *y*-coordinate (line) with 95% CI (gray shaded regions) over time for MVECs in the pH$_e$ gradient. The mean *y*-coordinate is significantly different than zero for all timepoints at which the error bars do not encompass the *x*-axis. (B) Mean *x*-coordinate (line) with 95% CI (gray shaded regions) over time for MVECs in the pH$_e$ gradient. The mean *x*-coordinate is not significantly different than zero at any timepoint. (C) Percentage of MVECs in the pH$_e$ gradient that attained a position with positive *y*-coordinate at the 8-h timepoint as a function of cell location within the gradient. No significant dependence on position was observed. (D) Mean MVEC velocity as a function of cell location within the gradient. Cells closer to pH$_e$ 7.5 moved significantly faster than those closer to pH$_e$ 6.0. Asterisk at location 1 indicates $p<0.05$ with respect to locations 2, 3, 4, and 5. Asterisk at location 2 indicates $p<0.05$ with respect to locations 4 and 5. Error bars are 95% CI.

could move toward acid even if the polarization direction is random and the cell velocity is independent of polarization direction.

However, simulation and experimental evidence suggest that this mechanism plays little, if any, role in our system. First, over the course of our 8-h experiments, individual $\alpha_v\beta_3$ CHO-B2 cells and MVECs traveled on average a distance less than 5% of the gradient width. Thus, over the limited region of the gradient that each cell explored over 8 h, cell velocity was approximately constant. We used simulations to further test this mechanism by making cell velocity dependent on *position* within the gradient but independent of migration *direction* (Fig. 3B). We accomplished this by eliminating integrin activation differences over the length of the cell in our migration model. Cell migration was then simulated for 100 cells with starting locations throughout the gradient and a randomized polarization direction at each time step. In these simulations, the mean cell position did not significantly move toward lower pH$_e$ within an 8-h timeframe (Fig. 3C). Taken together, these results suggest that it is unlikely that a chemokinetic trapping mechanism contributed significantly to causing the shift in mean cell position that we observed.

Cells move toward acidic regions due to increased migration velocity when polarized towards lower pH$_e$

Differential cell migration speeds toward versus away from acid constitutes a second potential mechanism for the shift in mean cell position toward acidic pH$_e$ (Fig. 3D). Based on the fact that pH$_e$ can regulate integrin activation [18], the percentage of activated integrins could be higher at one end of the cell than at the other in the presence of a pH$_e$ gradient. This asymmetry in adhesiveness between the leading and trailing ends of the polarized cell could in turn affect cell velocity. For a cell polarized with the leading edge toward lower pH$_e$, the gradient could enhance asymmetry in adhesiveness by activating leading edge integrins with greater frequency than trailing edge integrins, resulting in faster cell movement. The opposite effect could occur for cells polarized with the leading edge toward higher pH$_e$.

To test the effects of this potential mechanism, we performed similar simulations to those described above with the exception of allowing for pH$_e$-dependent integrin activation over the cell length. In these simulations, cells polarized toward lower pH$_e$ had greater velocities than those polarized in the opposite direction (Fig. 3E). As a result, the mean cell position was significantly greater than zero for most timepoints, even though the polarization direction was random (Fig. 3F). Thus, the model predicts that acid-induced integrin activation alone can lead to a shift in mean cell position toward lower pH$_e$, due to direction-dependent cell migration speed.

To assess the likelihood that this mechanism of direction-dependent velocity contributed to our results, we calculated the mean cell displacements in the direction of the gradient in our experiments (*y*-direction in Fig. 1B) over 1 h periods for cells migrating toward and away from acid within each of the five previously defined regions of the gradient (Fig. 3G and H). At most locations within the gradient, average migration speed was somewhat faster for cells migrating toward acid vs. away from acid, although at most positions within this gradient there

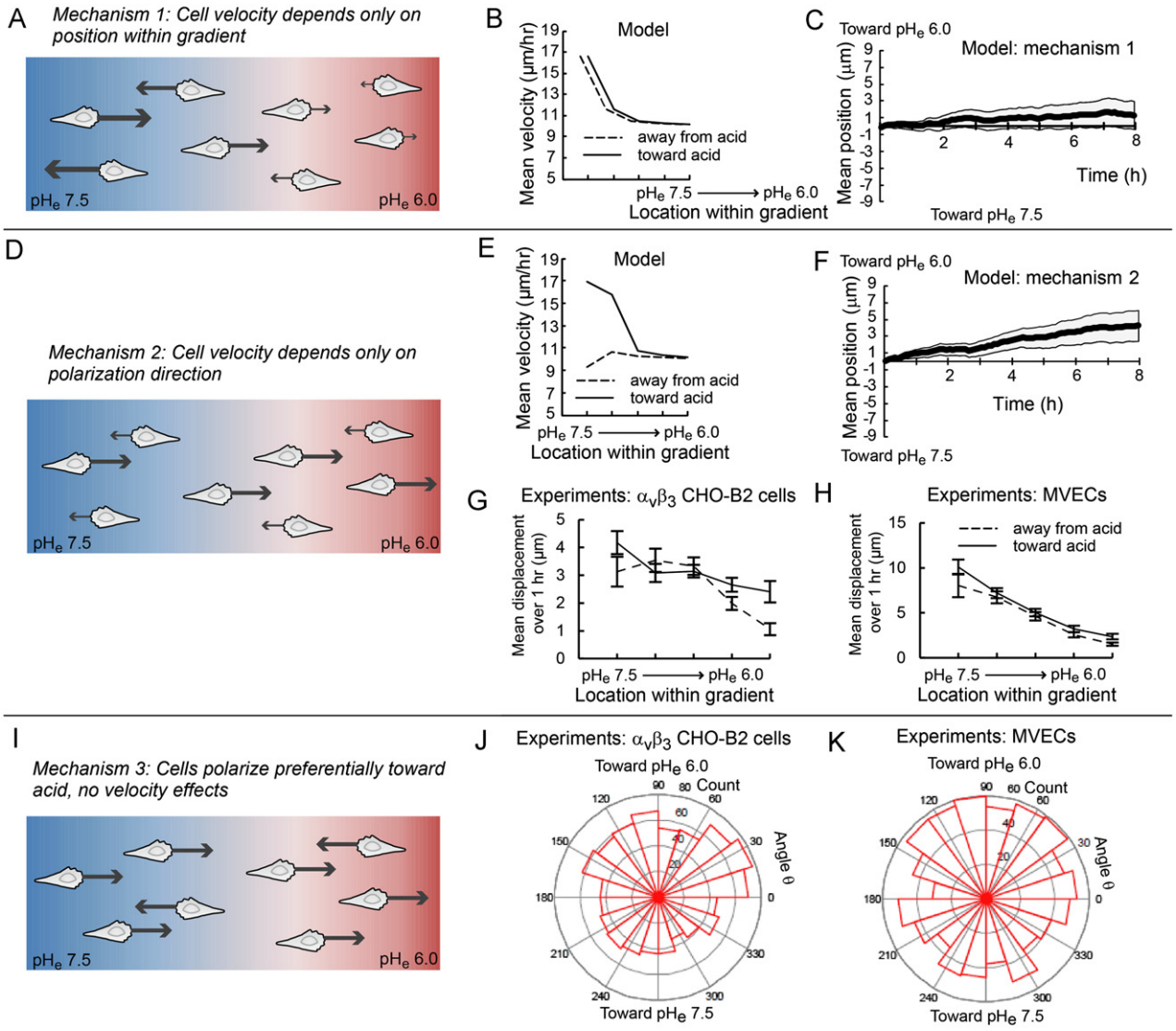

Fig. 3 – Three possible mechanisms for the shift in mean cell position toward acid over time. For A, D, and I, arrows indicate the magnitude of cell velocity, with larger arrows indicating higher speed. The direction of the arrows indicates the direction of polarization. Cell movement is restricted to one dimension for simplicity. (A) Mechanism 1: Cell velocity depends on the position within the gradient, decreasing for cells in more acidic positions. Cell velocity does not depend on polarization direction, and cells polarize equally in both directions. (B) Consideration of mechanism 1 with computational simulations: When the integrin activation rate is equal at the leading and trailing ends of the cell, there is no difference in velocity for a cell oriented toward acid (solid line) vs. away from acid (dashed line). Lines are offset for clarity. (C) In simulations testing mechanism 1, mean cell position (line) does not deviate significantly from zero within 8 h. (D) Mechanism 2: Cell velocity is higher for cells polarized toward acid, but velocity is independent of the position within the gradient and cells polarize equally in both directions. (E) Consideration of mechanism 2 with computational simulations: pH_e-dependent integrin activation across the cell length alters adhesion asymmetry between the two ends of the cell, leading to higher velocity toward vs. away from acid. (F) In simulations, mechanism 2 leads to a significant shift of the mean cell position (line) toward lower pH_e. (G and H) Experimental data comparing average $\alpha_v\beta_3$ CHO-B2 cell and MVEC velocities toward (solid line) and away (dashed line) from acid at different locations within the gradient. Error bars are the standard error of the mean. (I) Mechanism 3: Cells polarize preferentially toward acid, but cell velocity does not depend on polarization direction or position within gradient. (J) The angular distribution for $\alpha_v\beta_3$ CHO-B2 cells in the pH_e gradient is significantly different from a uniform distribution ($p = 2.4 \times 10^{-6}$). (K) The angular distribution for MVECs in the pH_e gradient is significantly different from a uniform distribution ($p = 0.0011$). Plots C and F from 100 simulations each for cells distributed throughout the gradient. Shaded regions are 95% CI.

was not a statistically significant level of difference ($p > 0.05$). For all gradient locations together, the average cell displacement toward acid was greater for both cell types: $\alpha_v\beta_3$ CHO-B2 cells displaced 3.08 ± 0.18 μm toward acid compared to 2.91 ± 0.14 μm away from acid, and MVECs displaced 5.82 ± 0.27 μm towards compared to 4.78 ± 0.29 μm away from

acid (all values mean ± SEM). This difference was not statistically significant ($p>0.05$) for the $\alpha_v\beta_3$ CHO-B2 cells, but was significant ($p=0.0084$) for the MVECs. Therefore, direction-dependent velocity may contribute to the net movement toward acid for the MVECs in our experiments, but this mechanism appears not to contribute significantly for the $\alpha_v\beta_3$ CHO-B2 cells. The difference between the two cell types implies that there are some cell-type specific differences in the mechanism of response to pH_e gradients, which may be related to variations in integrin expression or trafficking among different cell types.

Cells move toward acidic regions because of a preferential polarization towards lower pH_e

A third possible mechanism for the shift in mean cell position is illustrated in Fig. 3I. A pH_e gradient could cause a cell to alter its polarization direction by orienting the leading edge toward the more acidic end of the gradient. In other words, cells may polarize preferentially toward acid rather than polarizing with equal likelihood in all directions. By this mechanism of preferential orientation toward acid, the mean cell position could move toward acid independently of any velocity effects.

To assess whether cells preferentially polarized toward acid in our system, we analyzed angular histograms of our experimental cell displacement data, which display the distribution of angles (relative to the line perpendicular to the gradient) traversed for each 1-h segment of the cell trajectory (see Fig. S3F for methods). As these histograms take into account the displacement direction but not magnitude, they allow assessment of directional preference independently of any effects that the gradient has on cell speed. For $\alpha_v\beta_3$ CHO-B2 cells migrating in the gradient, the angular histogram demonstrates that positive angles of cell displacement were more common than negative angles, indicating directional bias toward the acidic end of the gradient (Fig. 3J). The Rayleigh statistical test indicates that this angular distribution significantly deviates from a uniform distribution ($p=2.4\times10^{-6}$). Similarly, for MVECs in the gradient, displacements with positive angles occurred more frequently than those with negative angles ($p=0.0011$), indicating directional preference toward lower pH_e (Fig. 3K). For both $\alpha_v\beta_3$ CHO-B2 cells and MVECs, angular histograms for cells in the control region did not indicate directional preference, with $p>0.05$ from the Rayleigh test (Fig. S3, G and H). Thus, these data demonstrate that $\alpha_v\beta_3$ CHO-B2 cells and MVECs in the pH_e gradient exhibited directional preference toward lower pH_e, indicating that this mechanism of preferential polarization is likely at least partially responsible for the shift in mean position toward acid that we observed.

Membrane protrusion dynamics and AIAC formation

Although the complete process underlying the directed polarization that we observed for both $\alpha_v\beta_3$ CHO-B2 cells and MVECs is likely complex and a full investigation is beyond the scope of this work, we aimed to further investigate two aspects of cell polarization that could be tied to acid-induced integrin activation. During cell migration, the cell membrane must protrude and form adhesions to the ECM or substratum. Membrane protrusion is often driven by actin polymerization, which is followed by integrin–ligand binding and formation of adhesion sites behind the leading edge [32]. At sites of integrin–ligand engagement, multi-protein assemblies called actin–integrin adhesion complexes (AIACs) form inside the cell, linking integrins to the actin cytoskeleton [33]. Alterations to membrane protrusion stability or AIAC development in acidic pH_e could cause cells to orient toward lower pH_e. To consider whether these two processes did indeed play a role in our studies, we measured the effects of acidic pH_e on membrane protrusion dynamics and AIAC formation for the model $\alpha_v\beta_3$ CHO-B2 cells.

We used kymography to measure cell membrane protrusion lifetime for $\alpha_v\beta_3$ CHO-B2 cells at pH_e 7.4 and 6.5. For these experiments, we imaged cells on fibronectin-coated glass at high magnification and high frequency to enable visualization of individual protrusion events and measurement of protrusion lifetime. The mean protrusion lifetime was significantly higher for cells at pH_e 6.5 vs. pH_e 7.4 (Fig. 4A), indicating increased stabilization of membrane protrusions in acidic pH_e.

To assess AIAC formation as a function of pH_e, we transfected $\alpha_v\beta_3$ CHO-B2 cells with GFP-vinculin. Transfected cells were plated on fibronectin-coated glass and exposed to pH_e 7.4 or pH_e 6.5 for either short timescales (20–40 min) or long timescales (2–3 h) before the mean number of AIACs per cell was

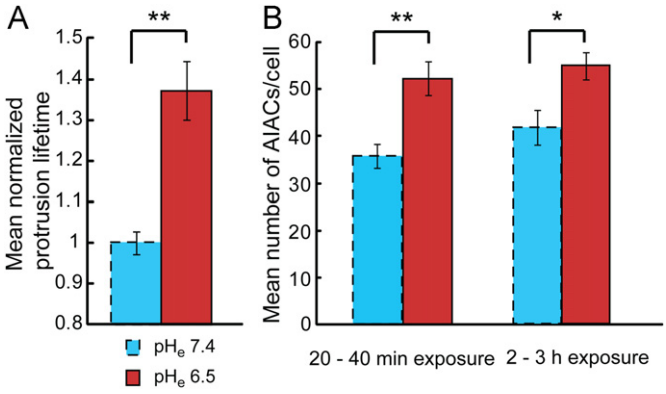

Fig. 4 – Membrane protrusion lifetime of $\alpha_v\beta_3$ CHO-B2 cells and number of AIACs/cell. (A) Average membrane protrusion lifetime for cells in $pH_e=6.5$ compared to that for control cells at $pH_e=7.4$. $^{**}p\leq0.0001$. Data are normalized to the average value for control cells tested on the same day. (B) Left two bars: Mean number of AIACs per cell for $\alpha_v\beta_3$ CHO-B2 cells exposed to pH_e 7.4 or 6.5 for 20–40 min. Right two bars: Mean number of AIACs per cell for $\alpha_v\beta_3$ CHO-B2 cells exposed to pH_e 7.4 or 6.5 for 2–3 h. $^{*}p<0.01$, $^{**}p<0.001$. Error bars are SEM.

measured. For short exposure times of 20–40 min, cells in pH_e 6.5 had significantly more AIACs/cell than cells in pH_e 7.4 (52.4±3.6 AIACs/cell and 35.8±2.5 AIACs/cell, respectively, mean±SEM, Fig. 4B). Similar results were observed with longer exposure times of 2–3 h (55.0±3.7 AIACs/cell and 41.9±2.9 AIACs/cell, respectively, mean±SEM, Fig. 4B). Thus, both short and long exposure to acidic pH_e increased the number of AIACs per cell compared to cells at pH_e 7.4.

Discussion and conclusions

In this study, to our knowledge we have demonstrated for the first time that cells can preferentially migrate toward acid in a pH_e gradient. This effect was observed for both model $\alpha_v\beta_3$ CHO-B2 cells and for MVECs, which are primary cells that express a physiologically relevant mixed population of integrins and are involved in healing and angiogenesis. While faster migration speeds toward versus away from acid may contribute somewhat to the migration towards acid, especially for the MVECs, preferential cell polarization towards acid appeared to be the dominant driving force in our experiments. Cells in acidic pH_e exhibited stabilized membrane protrusions and increased AIAC formation, hinting at possible mechanisms for the directed polarization that can now be explored further.

In a pH_e gradient, longer membrane protrusion lifetimes at the end of the cell exposed to more acidic pH_e could cause reorientation such that the acidic end of the cell becomes the leading edge. Increased formation of AIACs on membrane protrusions at this end of the cell could further reinforce this effect. In this manner, acidic pH_e could cause preferential cell polarization toward acid via alterations to subcellular-scale processes that are critical to migration. Our data show that the fraction of the cell population moving toward acid increases over time (Fig. S4), supporting our hypothesis of cellular reorientation toward acid upon exposure to a pH_e gradient.

Our computational simulations predict that the 1.5 pH unit gradient in pH over the channel used in our experimental studies is sufficient to cause integrin activation changes across the length of one cell. Although we did not measure protrusion lifetime or number of AIACs for cells within the gradient, other studies have demonstrated increased protrusion lifetimes [34] and larger numbers of AIACs [35] for cells plated on surfaces with higher fibronectin concentrations, as well as larger numbers of AIACs for cells interacting with ligands of higher binding affinity [36]. Small changes in the number of activated integrins between the leading and trailing cell edges could, in principle, cause small changes in protrusion lifetimes or number and size of AIACs; those changes could plausibly bias migration direction over time. The same effects could reinforce directed migration for cells with local cell surface pH_e gradients caused by NHE1 polarization [17], even if the overall environment has $pH_e \approx 7.4$. Though beyond the scope of this work, future studies could address protrusion and AIAC changes in pH_e gradients in more detail.

All of our results are consistent with a model of acid-induced integrin activation [18]. A larger number of activated integrins at the more acidic end of the cell could create more "traction" thus allowing cells to migrate faster when moving down a pH_e gradient. Too much binding, however, could slow cell migration; indeed, cells often exhibit biphasic migration speeds on substrates of increasing adhesiveness [18,27]. This could explain the decrease in migration speed in acidic regions exhibited by both the $\alpha_v\beta_3$ CHO-B2 cells and MVECs. Our cell migration model showed that integrin activation alone was sufficient to account for the position and direction-dependent velocities that we experimentally observed. Additionally, the increase in protrusion lifetime at pH_e 6.5 is consistent with increased integrin activation, which would be expected to lead to more efficient formation of nascent adhesion sites at the cell membrane, and would thus stabilize growing protrusions [18,34]. Increased intracellular AIAC assembly is also likely to be aided by increased integrin–ligand binding [33].

Our hypothesis is strengthened by the fact that we found that intracellular pH (pH_i) acidification, which can occur with acidic pH_e, to be insufficient to stabilize membrane protrusions (Supporting material and Fig S5). When pH_i was acidified for cells in a pH_e 7.4 bath by blocking the Na^+/H^+ ion exchanger NHE1 with EIPA, kymography measurements showed no increase in protrusion lifetime. It is also possible that intracellular acidification contributed to the changes in AIAC number that we observed. However, Srivastava et al. have shown that the number of AIACs in fibroblasts is independent of pH_i [37], which suggests that intracellular acidification is likely not sufficient to account for the changes to AIAC number that we observed at acidic pH_e. Although we did not experimentally test whether intracellular acidification affects the mechanism of direction-dependent migration velocity, our migration model demonstrates that this mechanism can occur without intracellular acidification. Thus, we posit that the shift in mean position of $\alpha_v\beta_3$ CHO-B2 cells and MVECs that we observed in migration experiments is mediated at least in part by pH_e. In support of our hypothesis, Klein et al. demonstrated that the migration of renal epithelial cells was independent of pH_i but depended on extracellular pH and the activity of NHE ion exchanger [23].

We note that the use of bicarbonate-free media introduces conditions depleted of HCO_3^- ions, which are present in physiological microenvironments. The absence of HCO_3^- may slow the rate of ion exchange and associated pH_i regulation that is dependent upon Na^+/HCO_3^- and Cl^-/HCO_3^- exchangers [23]. However, it has been demonstrated for different cell types that migration is independent of the presence on bicarbonate ions in the environment [21–23]. This lack of significant influence of bicarbonates on cell migration is in agreement with the demonstrated dominant role of the NHE exchanger in migration and not Na^+/HCO_3^- and Cl^-/HCO_3^- exchangers [17,21–23,38]. It is therefore unlikely that the observed directed cell migration in the pH_e gradient was an artifact of bicarbonate-free media use.

In addition to promoting integrin activation, acidic conditions could have effects directly on the fibronectin used to coat the plates in our experiments. We performed the fibronectin adsorption at pH_e 7.4, before the coverslips were exposed to a pH_e gradient, rendering it unlikely that the fibronectin concentration varied over the gradient length. Additionally, the fibronectin protein structure has been shown to be unchanged for $pH \geq 6.0$ [39,40]. However, we cannot completely rule out that pH-induced changes to fibronectin side chains affect the strength of integrin binding. If this were found to be the case, such effects of extracellular acidification could be yet another mechanism, in addition to those discussed above, influencing integrin-mediated migration in pH_e gradients.

Vascular endothelial cell migration toward acidic extracellular pH holds interesting implications for angiogenesis in the tumor and wound contexts. In wound healing, pH_e drops at 2–10 days post-injury [6,15]. This event coincides with the period in which vascular endothelial cells migrate into wounds [41]. As acidic pH_e is often correlated with hypoxia, this could serve as a signal directing cells toward regions where new blood vessels are especially needed. Thus, the acidic pH_e present in wound sites could help accelerate wound healing, and the same condition in tumors could accelerate tumor growth via angiogenesis. Interestingly, integrin $\alpha_v\beta_3$ is required for angiogenesis, and is upregulated on angiogenic endothelial cells [42]. One role of this integrin may be to act as a pH_e sensor and consequently direct endothelial cell migration toward acidic pH_e.

It is important to recognize that several molecular stimulators of angiogenesis, such as vascular endothelial growth factor (VEGF), are also regulated by pH_e. For example, acidic pH_e led to increased expression and secretion of VEGF in several human cancer cell lines [43–45], VEGF binding to endothelial cells and to fibronectin increased at acidic pH_e [46,47], and VEGF expression increased at acidic pH_e for brain tumors in vivo [43]. Several other angiogenic factors, such as interleukin 8, platelet-derived endothelial cell growth factor, and basic fibroblast growth factor, are also regulated by pH_e [48–50]. Furthermore, pH_e is not the only property of the cellular microenvironment that changes in the tumor and wound contexts. For example, it is well known that ECM stiffness increases at tumor sites, which can modulate integrin-dependent cell migration [51,52]. Thus, integrin activation in response to acidic pH_e is one of several ways in which extracellular stimuli could regulate cell migration and angiogenesis in the tumor and wound environments, and the interplay among various stimuli and responses is an interesting subject for future studies.

Acknowledgments

We thank A. Jagielska for insightful discussions on the manuscript. We gratefully acknowledge B. Geiger for the generous donation of the GFP-vinculin plasmid, as well as L. Griffith and I. Herman for providing cells. We also acknowledge funding support from the NSF CAREER Award (KJVV and RKP), the Singapore-MIT Alliance for Research & Technology (SMART) Biosystems & Micromechanics (BioSyM) Interdisciplinary Research Group via the Singapore NRF (KJVV, MJW, and RKP), R01 GM06966 (DAL), and the Siebel Scholar Award (RKP).

Appendix A. Supporting information

Supplementary data associated with this article can be found in the online version at http://dx.doi.org/10.1016/j.yexcr.2012.11.006.

REFERENCES

[1] J.L. Wike-Hooley, J. Haveman, H.S. Reinhold, The relevance of tumour pH to the treatment of malignant disease, Radiother. Oncol. 2 (1984) 343–366.
[2] R.J. Gillies, Z. Liu, Z. Bhujwalla, 31 P-MRS measurements of extracellular pH of tumors using 3-aminopropylphosphonate, Am. J. Physiol. Cell Physiol. 267 (1994) C195–203.
[3] G.R. Martin, R.K. Jain, Noninvasive measurement of interstitial pH profiles in normal and neoplastic tissue using fluorescence ratio imaging microscopy, Cancer Res. 54 (1994) 5670–5674.
[4] R.A. Gatenby, E.T. Gawlinski, A.F. Gmitro, B. Kaylor, R.J. Gillies, Acid-mediated tumor invasion: a multidisciplinary study, Cancer Res. 66 (2006) 5216–5223.
[5] L. Schneider, A. Korber, S. Grabbe, J. Dissemond, Influence of pH on wound-healing: a new perspective for wound-therapy?, Arch. Dermatol. Res. 298 (2007) 413–420.
[6] T.K. Hunt, P. Twomey, B. Zederfeldt, J.E. Dunphy, Respiratory gas tensions and pH in healing wounds, Am. J. Surg. 114 (1967) 302–307.
[7] A.J. Thistlethwaite, D.B. Leeper, D.J. Moylan Iii, R.E. Nerlinger, pH distribution in human tumors, Int. J. Radiat. Oncol. Biol. Phys. 11 (1985) 1647–1652.
[8] M.W. Dewhirst, R. Richardson, I. Cardenas-Navia, Y. Cao, The relationship between the tumor physiologic microenvironment and angiogenesis, Hematol./Oncol. Clin. N. Am. 18 (2004) 973–990.
[9] D.M. Prescott, H.C. Charles, J.M. Poulson, R.L. Page, D.E. Thrall, Z. Vujaskovic, M.W. Dewhirst, The relationship between intracellular and extracellular pH in spontaneous canine tumors, Clin. Cancer Res. 6 (2000) 2501–2505.
[10] O. Warburg, On the origin of cancer cells, Science 123 (1956) 309–314.
[11] J. Galarraga, D.J. Loreck, J.F. Graham, R.L. DeLaPaz, B.H. Smith, D. Hallgren, C.J. Cummins, Glucose metabolism in human gliomas: correspondence of in situ and in vitro metabolic rates and altered energy metabolism, Metab. Brain Dis. 1 (1986) 279–291.
[12] E. Bustamante, P.L. Pedersen, High aerobic glycolysis of rat hepatoma cells in culture: role of mitochondrial hexokinase, PNAS 74 (1977) 3735–3739.
[13] G. Helmlinger, F. Yuan, M. Dellian, R.K. Jain, Interstitial pH and pO2 gradients in solid tumors in vivo: high-resolution measurements reveal a lack of correlation, Nat. Med. 3 (1997) 177–182.
[14] H.H. Kühne, U. Ullmann, F.W. Kühne, New aspects on the pathophysiology of wound infection and wound healing—the problem of lowered oxygen pressure in the tissue, Infection 13 (1985) 52–56.
[15] T.K. Hunt, B. Zederfeldt, T.K. Goldstick, Oxygen and healing, Am. J. Surg. 118 (1969) 521–525.
[16] J.P. Remensnyder, G. Majno, Oxygen gradients in healing wounds, Am. J. Pathol. 52 (1968) 301–323.
[17] C. Stock, M. Mueller, H. Kraehling, S. Mally, J. Noël, C. Eder, A. Schwab, pH nanoenvironment at the surface of single melanoma cells, Cell. Physiol. Biochem. 20 (2007) 679–686.
[18] R.K. Paradise, D.A. Lauffenburger, K.J.Van Vliet, Acidic extracellular pH promotes activation of integrin $\alpha_v\beta_3$, PLoS One 6 (2011) e15746.
[19] D.S. Rhoads, J.L. Guan, Analysis of directional cell migration on defined FN gradients: role of intracellular signaling molecules, Exp. Cell Res. 313 (2007) 3859–3867.
[20] J.T. Smith, J.K. Tomfohr, M.C. Wells, T.P. Beebe, T.B. Kepler, W.M. Reichert, Measurement of cell migration on surface-bound fibronectin gradients, Langmuir 20 (2004) 8279–8286.
[21] A. Schwab, H. Rossmann, M. Klein, P. Dieterich, B. Gassner, C. Neff, C. Stock, U. Seidler, Functional role of Na+–HCO3− cotransport in migration of transformed renal epithelial cells, J. Physiol. 568 (2005) 445–458.
[22] C. Stock, B. Gassner, C.R. Hauck, H. Arnold, S. Mally, J.A. Eble, P. Dieterich, A. Schwab, Migration of human melanoma cells depends on extracellular pH and Na^+/H^+ exchange, J. Physiol. 567 (2005) 225–238.

[23] M. Klein, P. Seeger, B. Schuricht, S.L. Alper, A. Schwab, Polarization of Na^+/H^+ and Cl^-/Hco^{3-} exchangers in migrating renal epithelial cells, J. Gen. Physiol. 115 (2000) 599–608.
[24] B. Anand-Apte, B.R. Zetter, A. Viswanathan, R.G. Qiu, J. Chen, R. Ruggieri, M. Symons, Platelet-derived growth factor and fibronectin-stimulated migration are differentially regulated by the Rac and extracellular signal-regulated kinase pathways, J. Biol. Chem. 272 (1997) 30688–30692.
[25] L. Faff, C. Nolte, Extracellular acidification decreases the basal motility of cultured mouse microglia via the rearrangement of the actin cytoskeleton, Brain Res. 853 (2000) 22–31.
[26] R.B. Dickinson, R.T. Tranquillo, Optimal estimation of cell movement indices from the statistical analysis of cell tracking data, AIChE J. 39 (1993).
[27] P.A. DiMilla, K. Barbee, D.A. Lauffenburger, Mathematical model for the effects of adhesion and mechanics on cell migration speed, Biophys. J. 60 (1991) 15–37.
[28] M.R. Chernick, Bootstrap Methods: A Practitioner's Guide (Wiley Series in Probability and Statistics, Wiley-Interscience, 1999.
[29] D. Zicha, G.A. Dunn, A.F. Brown, A new direct-viewing chemotaxis chamber, J. Cell Sci. 99 (1991) 769–775.
[30] C.L. Schreiner, J.S. Bauer, Y.N. Danilov, S. Hussein, M.M. Sczekan, R.L. Juliano, Isolation and characterization of Chinese hamster ovary cell variants deficient in the expression of fibronectin receptor, J. Cell Biol. 109 (1989) 3157–3167.
[31] H. Enaida, T. Ito, Y. Oshima, T. Sakamoto, K. Yago, K. Kato, H. Kochi, Effect of growth factors on expression of integrin subtypes in microvascular endothelial cells isolated from bovine retinas, Fukushima J. Med. Sci. 44 (1998) 43–52.
[32] J.T. Parsons, A.R. Horwitz, M.A. Schwartz, Cell adhesion: integrating cytoskeletal dynamics and cellular tension, Nat. Rev. Mol. Cell. Biol. 11 (2010) 633–643.
[33] B. Geiger, A. Bershadsky, Assembly and mechanosensory function of focal contacts, Curr. Opin. Cell Biol. 13 (2001) 584–592.
[34] B.D. Harms, G.M. Bassi, A.R. Horwitz, D.A. Lauffenburger, Directional persistence of EGF-induced cell migration is associated with stabilization of lamellipodial protrusions, Biophys. J. 88 (2005) 1479–1488.
[35] S.L. Gupton, C.M. Waterman-Storer, Spatiotemporal feedback between actomyosin and focal-adhesion systems optimizes rapid cell migration, Cell 125 (2006) 1361–1374.
[36] M. Kato, M. Mrksich, Using model substrates to study the dependence of focal adhesion formation on the affinity of integrin–ligand complexes, Biochemistry 43 (2004) 2699–2707.
[37] J. Srivastava, G. Barreiro, S. Groscurth, A.R. Gingras, B.T. Goult, D.R. Critchley, M.J.S. Kelly, M.P. Jacobson, D.L. Barber, Structural model and functional significance of pH-dependent talin-actin binding for focal adhesion remodeling, PNAS 105 (2008) 14436–14441.
[38] G. Lauritzen, M. Jensen, E. Boedtkjer, R. Dybboe, C. Aalkjaer, J. Nylandsted, S.F. Pedersen, NBCn1 and NHE1 expression and activity in ΔNErbB2 receptor-expressing MCF-7 breast cancer cells: contributions to pH_i regulation and chemotherapy resistance, Exp. Cell. Res. 316 (2010) 2538–2553.
[39] A. Koide, M.R. Jordan, S.R. Horner, V. Batori, S. Koide, Stabilization of a fibronectin type III domain by the removal of unfavorable electrostatic interactions on the protein surface, Biochemistry 40 (2001) 10326–10333.
[40] B. Mallik, L. Zhang, S. Koide, D. Morikis, pH dependence of stability of the 10th human fibronectin type III domain: a computational study, Biotechnol. Progr. 24 (2008) 48–55.
[41] G. Broughton 2nd, J.E. Janis, C.E. Attinger, The basic science of wound healing, Plast Reconstr. Surg. 117 (2006) 12S–34S.
[42] P. Brooks, R. Clark, D. Cheresh, Requirement of vascular integrin alpha v beta 3 for angiogenesis, Science 264 (1994) 569–571.
[43] D. Fukumura, L. Xu, Y. Chen, T. Gohongi, B. Seed, R.K. Jain, Hypoxia and acidosis independently up-regulate vascular endothelial growth factor transcription in brain tumors in vivo, Cancer Res. 61 (2001) 6020–6024.
[44] L. Xu, D. Fukumura, R.K. Jain, Acidic extracellular pH induces vascular endothelial growth factor (VEGF) in human glioblastoma cells via ERK1/2 MAPK signaling pathway, J. Biol. Chem. 277 (2002) 11368–11374.
[45] Q. Shi, X. Le, B. Wang, J.L. Abbruzzese, Q. Xiong, Y. He, K. Xie, Regulation of vascular endothelial growth factor expression by acidosis in human cancer cells, Oncogene 20 (2001) 3751–3756.
[46] A.L. Goerges, M.A. Nugent, Regulation of vascular endothelial growth factor binding and activity by extracellular pH, J. Biol. Chem. 278 (2003) 19518–19525.
[47] A.L. Goerges, M.A. Nugent, pH regulates vascular endothelial growth factor binding to fibronectin, J. Biol. Chem. 279 (2004) 2307–2315.
[48] L. Griffiths, G.U. Dachs, R. Bicknell, A.L. Harris, I.J. Stratford, The influence of oxygen tension and pH on the expression of platelet-derived endothelial cell growth factor/thymidine phosphorylase in human breast tumor cells grown in vitro and in vivo, Cancer Res. 57 (1997) 570–572.
[49] Q. Shi, J.L. Abbruzzese, S. Huang, I.J. Fidler, Q. Xiong, K. Xie, Constitutive and inducible interleukin 8 expression by hypoxia and acidosis renders human pancreatic cancer cells more tumorigenic and metastatic, Clin. Cancer Res. 5 (1999) 3711–3721.
[50] D. D'Arcangelo, F. Facchiano, L.M. Barlucchi, G. Melillo, B. Illi, L. Testolin, C. Gaetano, M.C. Capogrossi, Acidosis inhibits endothelial cell apoptosis and function and induces basic fibroblast growth factor and vascular endothelial growth factor expression, Circulat. Res. 86 (2000) 312–318.
[51] M.J. Paszek, N. Zahir, K.R. Johnson, J.N. Lakins, G.I. Rozenberg, A. Gefen, C.A. Reinhart-King, S.S. Margulies, M. Dembo, D. Boettiger, D.A. Hammer, V.M. Weaver, Tensional homeostasis and the malignant phenotype, Cancer Cell. 8 (2005) 241–254.
[52] M.H. Zaman, L.M. Trapani, A.L. Sieminski, D. MacKellar, H. Gong, R.D. Kamm, A. Wells, D.A. Lauffenburger, P. Matsudaira, Migration of tumor cells in 3D matrices is governed by matrix stiffness along with cell-matrix adhesion and proteolysis, PNAS 103 (2006) 10889–10894.